[redacted]

NASA TECHNICAL MEMORANDUM

UB
NASA TM X-1328

COMPARATIVE STUDY OF RESULTS OBTAINED BY ANALYTICAL AND EXPERIMENTAL STRESS ANALYSIS FOR CIRCULAR PERFORATED PLATE

by Edward R. Hersman, William A. Bevevino, and Peter W. Verbulecz

Lewis Research Center
Cleveland, Ohio

NATIONAL AERONAUTICS AND SPACE ADMINISTRATION • WASHINGTON, D. C. • DECEMBER 1966

[redacted]

[redacted]

NASA TM X-1328

COMPARATIVE STUDY OF RESULTS OBTAINED BY ANALYTICAL AND EXPERIMENTAL STRESS ANALYSIS FOR CIRCULAR PERFORATED PLATE

By Edward R. Hersman, William A. Bevevino, and Peter W. Verbulecz

Lewis Research Center
Cleveland, Ohio

NATIONAL AERONAUTICS AND SPACE ADMINISTRATION

[redacted]

[redacted]

COMPARATIVE STUDY OF RESULTS OBTAINED BY ANALYTICAL AND EXPERIMENTAL STRESS ANALYSIS FOR CIRCULAR PERFORATED PLATE (U)

by Edward R. Hersman, William A. Bevevino, and Peter W. Verbulecz

Lewis Research Center

SUMMARY

The reactor support plate is a primary structural member of the nuclear rocket reactor, and the work reported herein was conducted to determine the degree of accuracy of presently available design methods when used to predict the mechanical behavior of the reactor support plate. The reactor support plate was centrally loaded, and strains were measured at various locations on the plate. The experiment was conducted for one magnitude of load only, and the experimental strains were compared with strains calculated by presently available analytical methods. The two methods of analysis used to calculate the strain levels in the plate were a ligament-efficiency method based on geometry change and a materials-property-change method.

The calculated strains, when compared with those measured, indicated that the ligament-efficiency method more closely approximated the experimental results than the materials-property-change method. At a radial distance of 10 inches and for the case neglecting friction at the supports the ligament-efficiency method gave tangential strains approximately 50 microinches per inch (22 percent) greater than the measured strains, whereas the materials-property-change method gave tangential strains approximately 150 microinches per inch (67 percent) greater than the measured strains. At a radial distance of 8 inches, the calculated strains differed from the measured strains by as much as 91 percent.

INTRODUCTION

The analytical and experimental work contained herein was undertaken as part of an overall reactor structures program. A nuclear rocket consists of many components, and

[redacted]

the reactor components are interlocked in such a fashion that, if load is applied on any one component, there is an effect, to a variable degree, on all other components in the system. System stress analysis of a structure such as a nuclear rocket reactor requires the simultaneous evaluation of each component under its individual load profile, together with loads or constraints which may be transferred to it from adjacent components. The values of loads or constraints as imposed by neighboring components are generally of a statically indeterminate nature and can be obtained only through the solution of a large matrix. This matrix frequently consists of equations which express the fact that all loads on each component must be in equilibrium and that certain relations regarding motion must be maintained at points where the components are in conjunction.

The core support plate is a primary structural member of a nuclear rocket reactor. The loads imposed on this plate consist of those due to pressure drop, to temperature distribution, and to the neighboring components; the loads due to the neighboring components are statically indeterminate. The thermal loading, resulting from temperature distribution, was not considered in this work, since once the behavior of the reactor core under ambient pressure loads has been established and can be predicted, then the thermal effects can be considered. The true stress and displacement of the plate can be obtained, provided that analytical methods which are capable of determining these quantities under all possible reactor load conditions are available. The analysis and experiment reported herein was conducted to determine the feasibility of using analytical methods which are presently available for accurately evaluating stress and strain in a plate of this type.

Perforated circular plates (tube sheets) are widely used in heat exchangers, and practically all past experimental and analytical endeavors have used tube sheets as models. Tube sheets are generally perforated with holes of equal diameter, which are so located that their centers form equilateral triangles. Being somewhat empirical by nature, the analytical stress methods which were developed for tube sheets are highly restrictive and cannot accurately be used for plates perforated with nonuniform diameter holes or where the pitch between the holes is a variable.

The test and the analysis reported herein were made to determine the degree of accuracy of presently available design methods and to provide a basis for new analytical methods. Generally, the test consists of loading the support plate with a predetermined load and monitoring the strains with strain gages. The experiment is explained in more detail in the TEST PROCEDURE section. The strains were calculated by means of available analytical methods, and these theoretical strains were compared with the measured ones.

Two methods of analysis were employed: a ligament-efficiency method and a materials-property-change method. A bracket type of analysis, based on the thickest and the thinnest ligaments in the plate, was employed. The analysis involving the thinnest ligament (cases A-2 and B-2) should yield strain levels higher than those measured;

the analysis involving the thickest ligament (cases A-1 and B-1) should yield strains of lesser magnitude. A failure to obtain calculated strain values which are both higher and lower than the measured strains would mean that the present methods of analysis are overly conservative, and any modification of the methods to fit the variable flexural rigidity of the plate would be difficult, if not impossible.

TEST SPECIMEN

The test specimen was a 6061-T6 aluminum forging and consisted of a circular reactor support plate 39.875 inches in overall diameter (fig. 1). The basic pattern of the holes in the plate consisted of a tie-rod hole surrounded by a circular pattern of six flow holes (fig. 2). The reactor core was suspended by tie rods which fit into the tie-rod holes. The flow holes were of a constant diameter, 0.502 inch, and these holes penetrated the thickness of the plate. For 3.5 inches of the plate thickness the tie-rod holes have diameters of 0.625 inch, and the remainder of the tie-rod-hole penetration is oblong (fig. 2). The plate area inscribed by a circle with a 17.65-inch radius (figs. 1 and 3) was almost completely perforated. The outer periphery of this area was drilled with holes in a random pattern; hence, the flow-hole - tie-rod-hole pattern could not be regarded as general. A bevel was cut at the top of the plate near the edge of the perforated section as shown in figure 3.

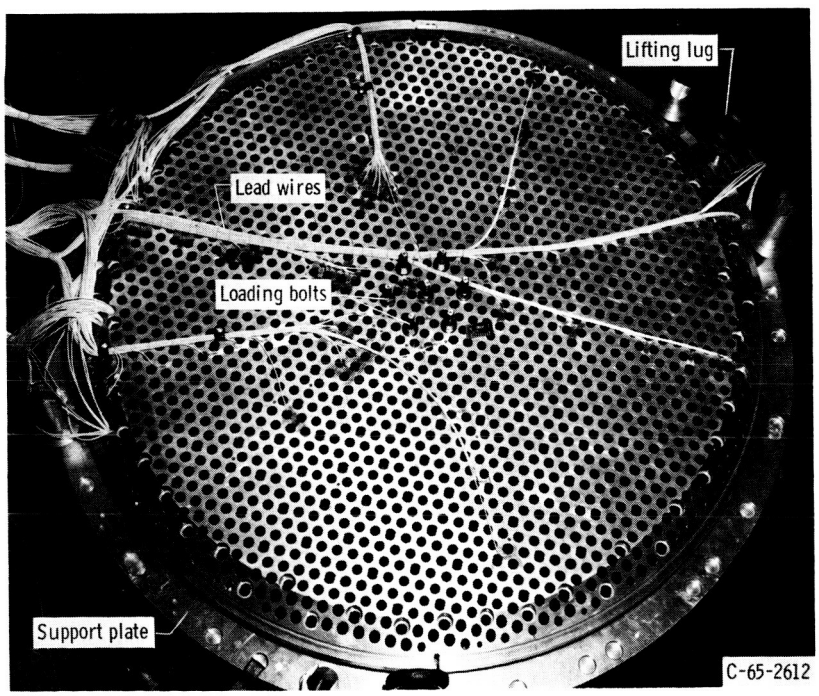

Figure 1. - Reactor support plate.

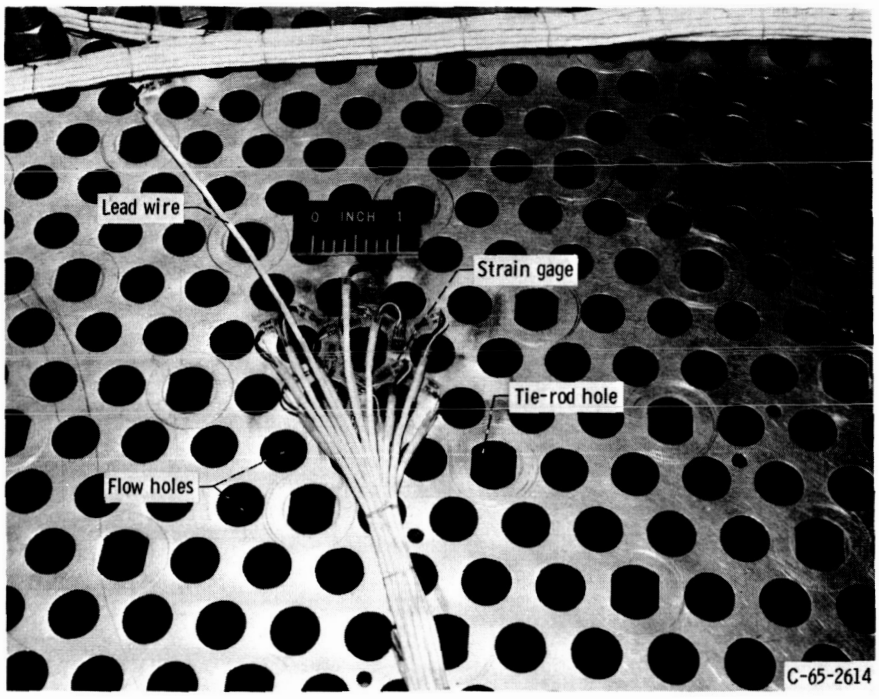

Figure 2. - Basic pattern of flow holes and tie-rod holes.

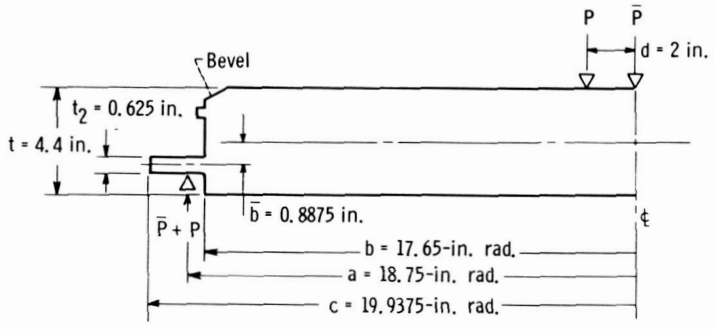

Figure 3. - Support plate loads and external dimensions.

TEST PROCEDURE

The loading and strain gaging of the plate was to furnish data for comparison with analytical results. The loading fixture consisted, as shown in figure 4, of a cylinder with a stay plate welded near the bottom. The support plate rested on the rounded edges of the cylinder top, and the reactor support plate was loaded by elongating seven centrally located bolts to a predetermined strain level. The bolts were strain gaged at 120^{o} increments around the circumference at the same elevation, so that the effect of any direct load could be isolated from the bending effects. A load of a predetermined amount was generated by tightening the bolts to the desired strain level.

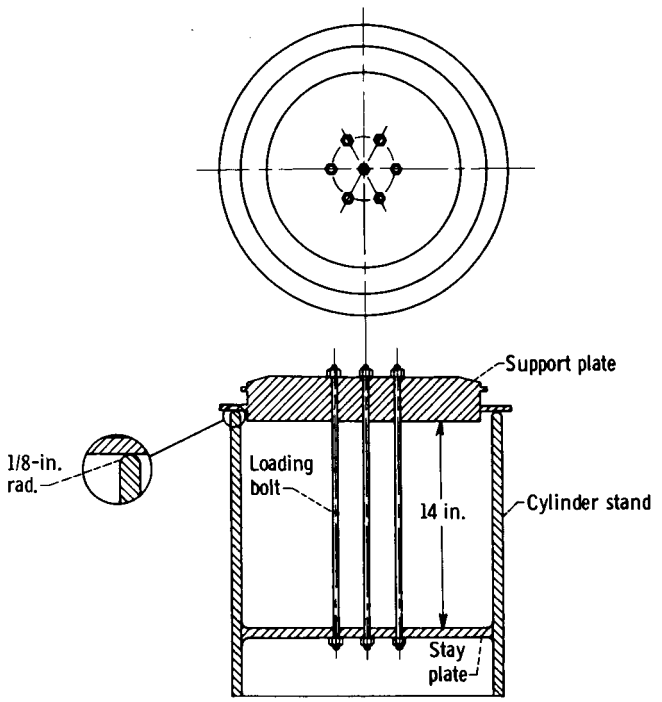

Figure 4. - Test fixture and support plate.

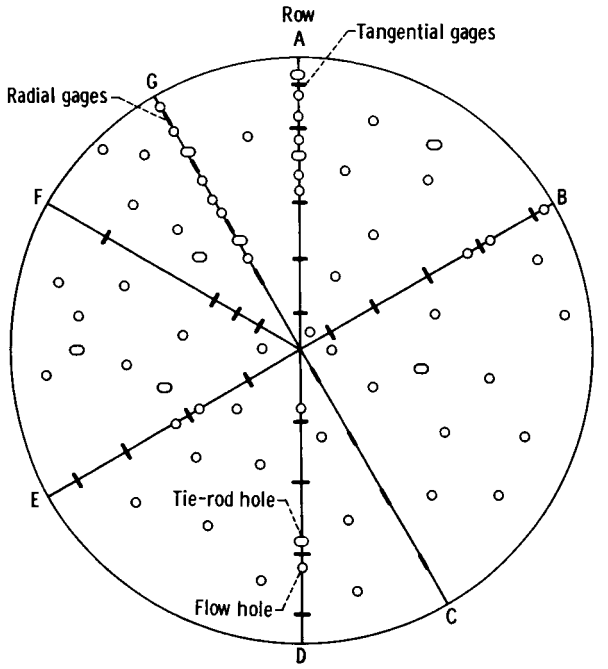

Figure 5. - Schematic view of strain-gage radial and tangential orientation.

The strain gages were placed at the top and the bottom of the support plate directly across the thickness from each other. The general pattern of the strain gages can be seen in figure 5; only those holes which are necessary to describe the tangential and radial patterns are shown. The first analytical check against gage readings was for tangential and radial strains. Figure 5 shows that the gages in rows A, C, D, E, F, and G were located so these strains could be read directly. The strain gages in row B were placed in a pattern which would give an indication of strain within a particular hole pattern. Gages were also placed on ligaments which were neither tangentially nor radially oriented; these gages were intended to measure the vector effects from both directions. Several rows of gages which would seemingly duplicate readings were used (rows A, B, D, and E, fig. 5), since it was assumed that the plate might not be axisymmetrical and a cross-checking of readings would be desirable.

Before the load was applied to the support plate, the reading of each gage was recorded. The support plate was then loaded, and gage readings were again recorded. A final set of strain-gage readings was taken immediately after the applied load was released. This procedure was followed for every test run. For each test run, the total load applied to the support plate was 30 246 pounds, and readings were recorded for only this magnitude of load. The experimental data are presented in table I.

TABLE I. - EXPERIMENTAL AND ANALYTICAL STRAINS

(a) Tangential strains

Position	Experimental data			Calculated strain, μin./in.							
	Gage	Radius, in.	Readings, μin./in.	Friction free				Friction locked			
				Case A-1 (thick-ligament, property-change method)	Case A-2 (thin-ligament, property-change method)	Case B-1 (thick-ligament, ligament-efficiency method)	Case B-2 (thin-ligament, ligament-efficiency method)	Case A-1 (thick-ligament, property-change method)	Case A-2 (thin-ligament, property-change method)	Case B-1 (thick-ligament, ligament-efficiency method)	Case B-2 (thin-ligament, ligament-efficiency method)
Top	A12	13.38	-145	-210	-278	-204	-261	-209	-276	-203	-268
	A9	9.50	-214	-278	-372	-268	-347	-277	-371	-268	-354
	A3	4.19	-408	-431	-584	-412	-537	-430	-582	-412	-544
	D4	14.25	-129	-197	-260	-192	-245	-196	-259	-191	-252
	D3	11.75	-176	-236	-314	-228	-294	-235	-313	-228	-301
	D2	8.00	-264	-312	-419	-300	-389	-311	-418	-300	-396
	D1	4.25	-404	-428	-580	-410	-534	-427	-579	-410	-541
Bottom	A12	13.38	139	206	271	201	257	203	266	198	258
	A9	9.50	210	275	366	266	342	271	361	262	343
	A3	4.19	394	427	577	410	532	424	572	406	534
	D4	14.25	97	193	254	189	241	190	249	185	242
	D3	11.75	152	232	307	226	289	229	303	222	291
	D2	8.00	245	308	413	298	384	305	408	294	386
	D1	4.25	390	424	574	407	530	421	569	404	531

(b) Radial strains

Top	G11	16.50	-40	36	63	28	46	37	64	29	39
	G9	13.88	-91	.13	13	-6.0	.92	.78	14	-5.0	-6.1
	G8	11.25	-162	-44	-48	-47	-54	-43	-47	-47	-62
	G7	9.88	-171	-72	-86	-74	-89	-71	-85	-73	-96
	G6	8.62	-211	-101	-127	-101	-125	-100	-126	-100	-132
	G5	7.25	-260	-139	-179	-137	-172	-138	-178	-136	-179
	G4	6.00	-309	-181	-283	-177	-225	-180	-236	-176	-232
	C5	15.25	-73	20	40	13	25	20	41	14	18
	C4	12.50	-125	-22	-17	-26	-27	-21	-16	-26	-34
	C3	9.88	-171	-72	-86	-74	-89	-71	-85	-73	-96
	C2	7.25	-258	-139	-179	-137	-172	-138	-180	-136	-179
	C1	3.25	-384	-331	-445	-318	-412	-330	-444	-318	-419
Bottom	G11	16.50	84	-38	-70	-31	-50	-43	-74	-35	-49
	G9	13.88	82	-2.0	-20	3.0	-5.3	-6.8	-24	-.8	-3.8
	G8	11.25	160	42	42	45	50	37	37	41	51
	G7	9.88	174	70	80	71	84	65	75	67	86
	G6	8.62	214	99	120	98	121	94	116	95	122
	G5	7.25	271	137	173	134	168	132	168	130	169
	G4	6.00	276	179	232	174	221	174	226	170	221
	C5	15.25	72	-22	-47	-15	-30	-26	-51	-19	-28
	C4	12.50	111	20	11	24	22	15	6.3	19	24
	C3	9.88	159	70	80	71	84	65	75	67	86
	C2	7.25	----	137	173	134	168	132	168	130	169
	C1	3.25	----	329	439	316	408	324	434	312	409

INSTRUMENTATION

The strain gages used in the test were foil-type units with a gage factor of 2.00, a resistance of 120 ± 0.2 ohms, a width of 0.067 inch, and a length of 0.062 inch. The thermal expansion characteristic of the strain gages was matched to that of the plate. For the 6061-T6 aluminum support plate material, the thermal compensation of the gage was 12 parts per million per degree Fahrenheit. The recommended allowable strain for the gages is 2 percent of its length, and this value was never exceeded during the test. A total of 158 gages were used, and, in general, the gages were positioned with the gage length parallel to the length of the ligament.

The strain gages were bonded to the plate with cyanoacrylate cement and were moistureproofed with nitrile rubber emulsion. The cyanoacrylate cement used was cause for concern during the test, since time stability could be a problem, and approximately 2 months had passed between the application of the gages and the actual test. The repeatability of the gage readings showed that the time stability limit of the cement had not been exceeded. The polymerized cyanoacrylate cement used is limited to elongations of the order of 2 to 3 percent at room temperatures. This limitation was never exceeded in the test; hence, brittle cracking was not a problem.

The lead wire used for the strain-gage installations was 30-gage wire (0.012-in. diam) with a twisted and braided wire shield and a resistance of 1 ohm per 10 feet of length. The gage leads used for the test were 10 feet long. The strain gages were isolated from ground by at least 35 megohms, and the system used a single, heavy point ground, carried throughout by the shield of the wires.

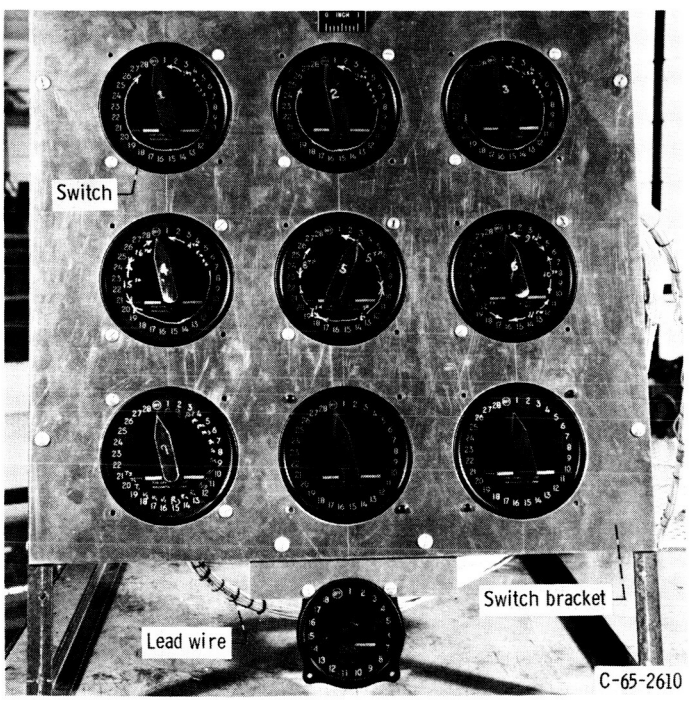

Figure 6. - Front view of switching panel.

The indicating instrument was a Baldwin-Lima-Hamilton strain-gage indicator model 120. Each pair of strain-gage signals was transferred with high-quality, extremely low-resistance thermocouple-type switches (fig. 6).

A criterion for establishing the reliability of the readings was that the reading of each gage after the load was released had to be equal to within ±10 microinches per inch of the initial unloaded reading. Many readings were eliminated from the

valid data by this criterion.

STRESS ANALYSIS

The analyses herein described use the concept of a solid equivalent plate. This concept is based on the premise that a perforated plate can be analyzed by classical methods which are utilized to evaluate solid plates if certain adjustments are made to its rigidity or its material properties. Two widely accepted methods of analysis were used. In one method, the flexural rigidity of a solid plate with the same dimensions as those of the perforated plate is reduced by use of a ligament-efficiency factor which accounts for the holes. The cases reported herein which employ this method of analysis are designated B-1 and B-2. Case B-1 is concerned with the thickest ligament, and case B-2 deals with the thinnest ligament (fig. 7). In the other method of analysis, the solid equivalent plate has the same dimensions as the perforated plate, but the true modulus of elasticity and Poisson's ratio are replaced by fictitious values. The cases dealing with this method of analysis are designated A-1 and A-2. Case A-1 is concerned with the thickest ligament, and case A-2 deals with the thinnest ligament.

In the field of perforated plate design, major contributions have been made by the following authors: Horvay (ref. 1), Gardner (ref. 2), Miller (ref. 3), Duncan (ref. 4), Sampson (ref. 5), and Leven (ref. 6). Practically all their work, however, has been restricted to plates with holes of equal diameter arranged in an equilateral triangular system. Methods for analyzing single oversize or misdrilled holes, which are located among those of equal diameter and with the equilateral triangular pattern, are available in a paper by O'Donnell and Langer (ref. 7). Two general conditions, relating to the loads generated at the plate support, were analyzed: (1) The plate is simply supported and the frictional effects between the support cylinder and plate are negligible (friction-free condition), and (2) the plate and the support cylinder move radially together because of friction effects (friction-locked condition).

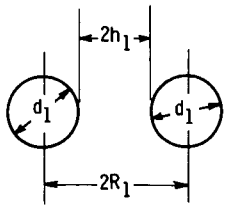

(a) Flow hole to flow hole.

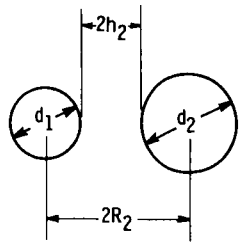

(b) Flow hole to bolt hole.

Figure 7. - Ligaments.

In the evaluation, the plate was assumed to be cut into two components, as shown in figure 8(a). The components were evaluated individually for slope and radial displacement at their common junctures in terms of the known external loads and unknown internal forces at the juncture as shown in figure 8. The algebraic statement that the slope and the radial displacement at common junctures must be the same leads to a matrix, and the solution of the matrix yields values for the statically indeterminate loads. The substitution of

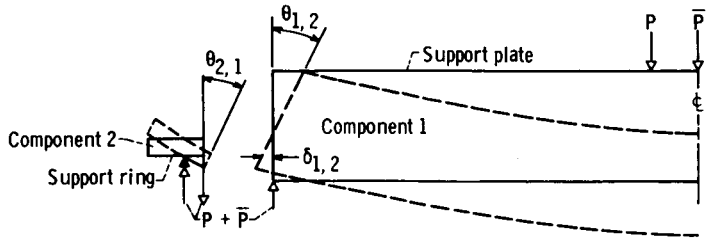

(a) Friction-free condition; known loads.

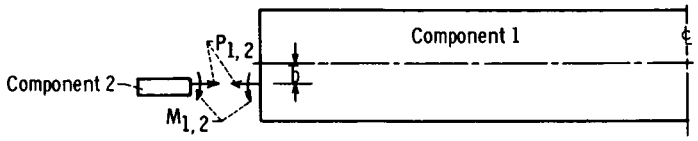

(b) Friction-free condition; statically indeterminate loads.

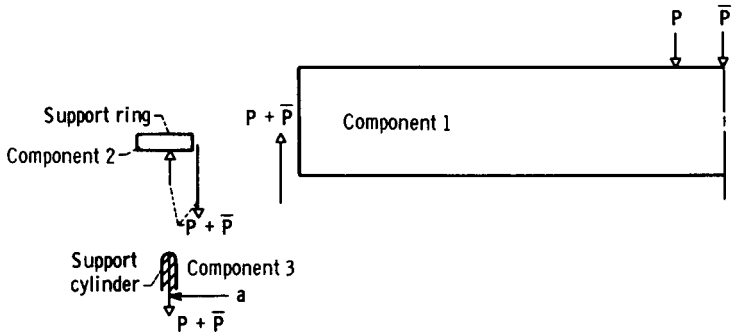

(c) Friction-locked condition; known loads.

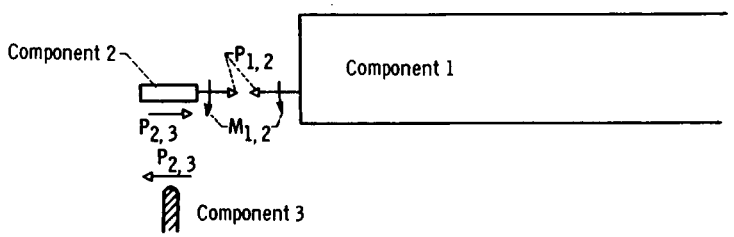

(d) Friction-locked condition; statically indeterminate loads.

Figure 8. - Known and statically indeterminate loads.

these values into previously derived strain equations yields values for comparison against measured strains.

Practically all the basic terms used in the matrix equations and for the strain evaluation are available from the literature. To determine the feasibility of present methods of analysis, a bracket type of analysis was used. The bracket analysis consists of two parts: The first part involves only the thinner ligaments (cases A-2 and B-2), while the second part involves only the thicker ligaments (cases A-1 and B-1). Cases A-2 and B-2 should yield strain levels higher than those measured, while cases A-1 and B-1 should

yield values lower than actuality.

The failure of the analytical strain curves to bracket the measured strains would cast doubt on the methods of analysis, since any adjustment of rigidity to account for the different size holes would cause strain levels to fall between these two extremes. The symbols used throughout the analysis are presented in appendix A, and the complete analytical solution for the plate is in appendix B.

RESULTS

The gages, which were placed inside holes of the plate, failed to return to zero when the load was removed from the plate; hence, any valid experimental verification of the stress intensification factor used in the analysis was eliminated. The comparative strain levels presented herein are based on a stress-intensification factor of 1. A stress-intensification factor of 1 yields calculated stress values of the smallest possible magnitude for the existing load condition. If a stress-intensification factor greater than 1 were used, the calculated stresses would have been of a greater magnitude than those presented herein.

Plots of the calculated and the measured strains are presented in figure 9. For all the plots, the abscissa is the radial distance from the center of the plate, and the ordinate is the corresponding strain at the various radial locations. Five curves are presented on each graph: (1) the experimental data, (2) the materials-property-change method based on the thickest ligament (case A-1), (3) the materials-property-change method based on the thinnest ligament (case A-2), (4) the ligament-efficiency method based on the thickest ligament (case B-1), and (5) the ligament-efficiency method based on the thinnest ligament (case B-2). Figures 9(a) to (d) are for the friction-free condition, and figures 9(e) to (h) are for the friction-locked condition.

In the plotting of figure 9, only the strains pertinent to ligaments between flow holes were considered. A row of radial gage readings, if plotted in their entirety, would indicate a substantial amount of scatter. This scatter is easily explained, since the strain levels for the thin ligaments should be higher than those for the thicker ligaments. Strain-gage readings which did not return to 0 when the plate was unloaded were eliminated from the plotted data.

The comparison of the strains obtained by analysis with those obtained from measurements, as shown in figure 9, produced the following facts:

(1) Regardless of the ligament or the condition assumed for the plate, the analytical strains were always higher in the tangential and lower in the radial directions than those measured.

(2) The older ligament-efficiency method of analysis yielded strain levels, in most

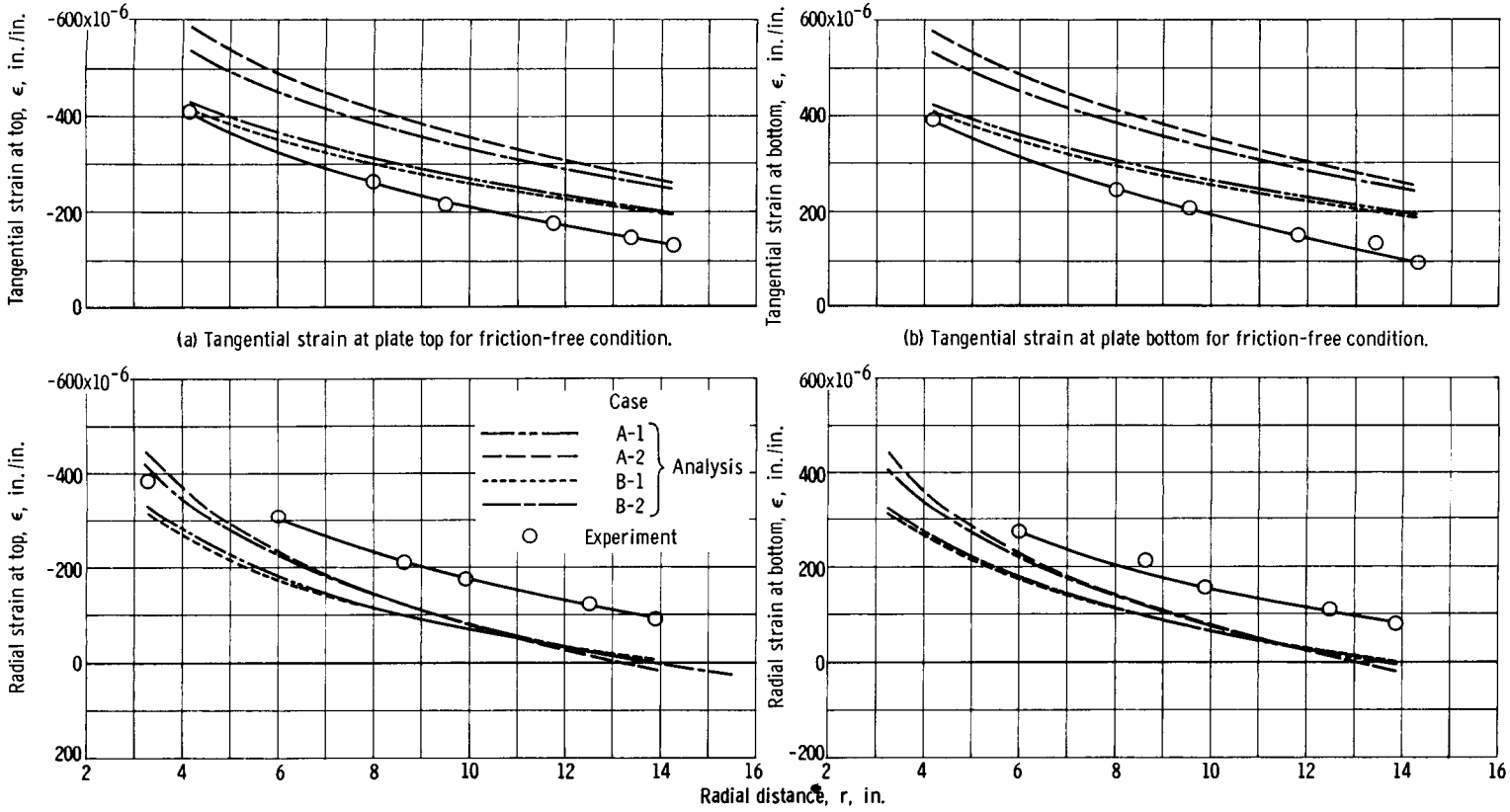

(a) Tangential strain at plate top for friction-free condition.

(b) Tangential strain at plate bottom for friction-free condition.

(c) Radial strain at plate top for friction-free condition.

(d) Radial strain at plate bottom for friction-free condition.

Figure 9. - Experimental and analytical strain as function of radial distance.

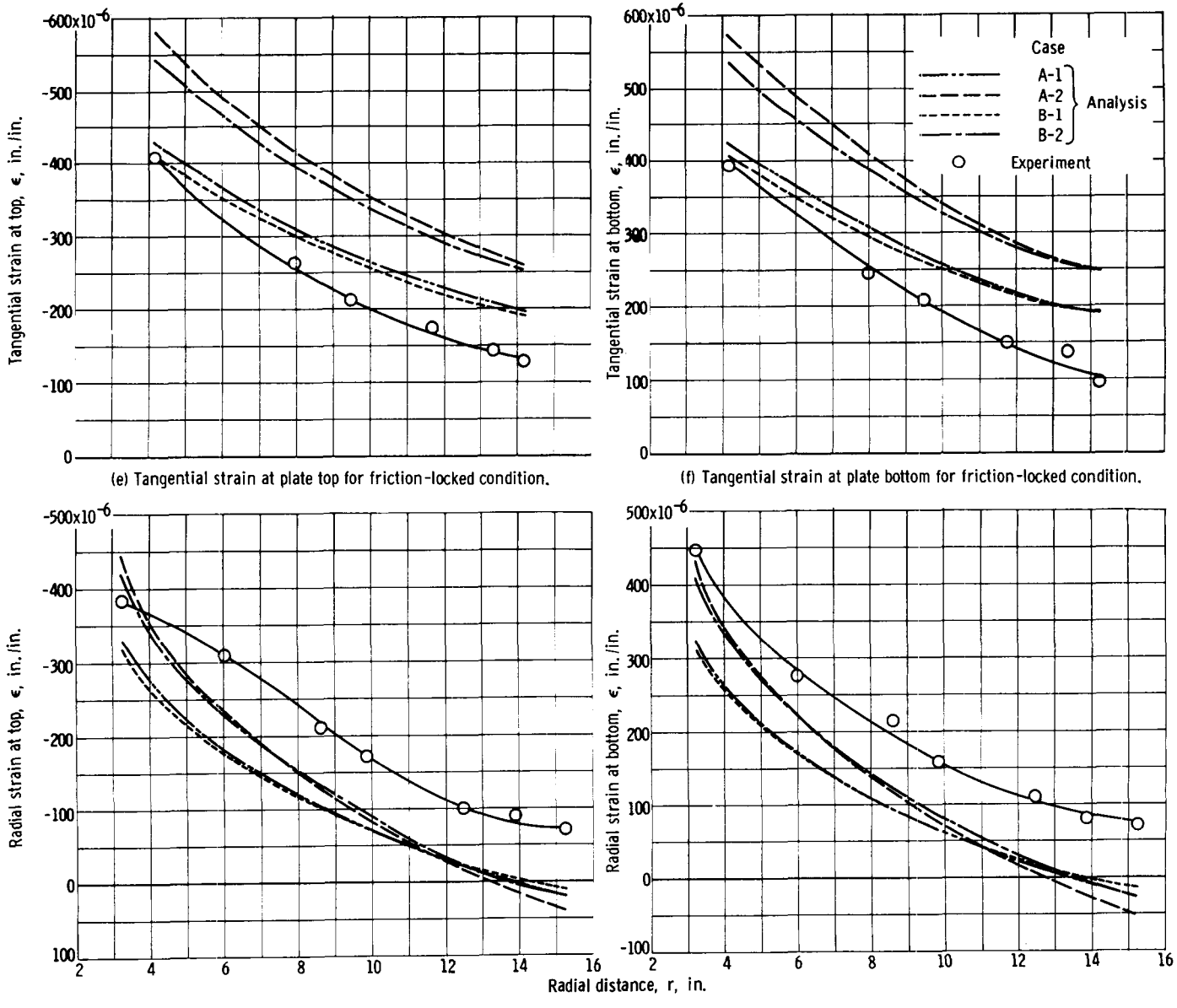

(e) Tangential strain at plate top for friction-locked condition.

(f) Tangential strain at plate bottom for friction-locked condition.

(g) Radial strain at plate top for friction-locked condition.

(h) Radial strain at plate bottom for friction-locked condition.

Figure 9. - Concluded.

cases, nearer to those measured than did the material-property-change method. For the friction-free condition and at a radial distance of 5 inches, the ligament-efficiency method (case B-2) gave strains approximately 125 microinches per inch (34 percent) greater than the measured strains, whereas the materials-property-change method (case A-2) gave strains approximately 175 microinches per inch (48 percent) greater than the measured strains (fig. 9(a)).

(3) In general, the two methods of analysis used to calculate the analytical strains yielded results which were of practically the same magnitude. For all the conditions reported herein, the difference observed between the two methods of analysis never exceeded 10 percent, and this percentage difference existed near the plate center only (figs. 9(c) and (d)).

(4) The analysis indicated that there should be a sign change in radial strain near the edge of the perforated portion of the plate. At a radial distance of approximately 13 inches and for all four analytical conditions (cases A-1, A-2, B-1, and B-2), the radial strain exhibited a sign change, but this sign change was not indicated by the experimental data (figs. 9(g) and (h)).

(5) The analytical strains near the plate center were closer to those measured than the analytical strains near the plate edge. As shown in figure 9(e) for case B-1, the measured strain was equal to the calculated strain at a radial distance of 4 inches, whereas the calculated strain was 44 percent greater than the measured strain at a radial distance of 14 inches. Similar results are shown in figures 9(a) and (b).

(6) In general, the analytical strain curves had the same shape as the measured strain curves.

(7) The plate exhibited only small indications of asymmetry (fig. 9).

(8) The frictional effect induced by the action of the radial loading from the support plate on the cylinder was of negligible significance. The analytical results of the friction-free condition gave values which differed from the results of the friction-locked condition by approximately ±2 percent.

CONCLUSIONS

A comparative study was made of results obtained by analytical and experimental stress analysis for a circular perforated plate. Because the ligament-efficiency method of analysis yielded strain values which are closer to those measured than the material-property-change method did, and the difference between the results of the two methods of analysis is relatively small, the older and simpler efficiency method should be used in plate design until more advanced analytical methods are developed.

Notwithstanding further development work, the following conclusions were drawn:

1. The present methods of analysis are adequate for predicting stress levels near the plate center, but any analysis which involves constraints around the outer periphery of the plate will be erroneous.

2. There is little advantage to be gained in the use of the more cumbersome material-property-change type of analysis, for the older and simpler ligament-efficiency method is apparently more applicable.

3. The deviation of the calculated strains from the measured strains, together with the failure of the radial measured strain to change sign near the plate edge, tends to cast doubt on the accuracy of analyses which assume that a perforated plate can be calculated as an equivalent solid plate. The failure to bracket the actual strains analytically by assuming (1) that the plate consisted completely of the stiffer ligaments, and (2) that it consisted completely of the more flexible ligaments, indicates that any variable stiffness used between these two extremes would be invalid. The failure of the measured strains to reverse sign indicates that the plate is not in a complete biaxial stress field, as the equivalent solid plate type of analysis would indicate. Thus, improved methods of analysis are needed if accuracy is of significant importance in the design.

Lewis Research Center,
National Aeronautics and Space Administration,
Cleveland, Ohio, August 15, 1966,
122-29-04-10-22.

APPENDIX A

SYMBOLS

A	area, sq in.
a	radius of plate support, in. (fig. 3)
b	radius of perforated section of plate, in. (fig. 3)
$\overline{b}$	axial length between deflection surfaces of components 1 and 2, in.
c	radius of support ring, in.
D	$Et^3/12(1 - \nu^2)$, lb-in.
d	radial distance to load bolts, in.
d_1	diameter of flow hole, in.
d_2	diameter of bolt hole at plate bottom, in.
d_3	average diameter of two holes bounding ligament, in.
E	modulus of elasticity, psi
h	one-half of any ligament width, in.
h_1	one-half of ligament width between flow holes, in.
h_2	one-half of ligament width between flow hole and bolt hole, in.
K	efficiency factor, $(2R - d_3)/2R$
$\overline{K}$	foundation modulus of support cylinder, lb/in.
M	moment, in.-lb/in.
P	load generated by six bolts on plate, lb
$\overline{P}$	load generated by center bolt on plate, lb
P_x	pressure load on subring 2B, psi (fig. 10)
R	one-half distance between holes, in.
R_1	one-half distance between flow holes, in.
R_2	one-half distance between bolt hole and flow hole, in.
r	radial distance, in.
t	thickness, in.
t_2	support ring thickness, in. (fig. 3)
Y	stress intensification factor
$\delta_{1,2}$	radial displacement of component 1 at its juncture with component 2, in.
$\delta_{2,1}$	radial displacement of component 2 at its juncture with component 1, in.
$\delta_{2,3}$	radial displacement of component 2 at its juncture with component 3, in.
$\delta_{3,2}$	radial displacement of component 3 at its juncture with component 2, in.

[redacted]

ϵ	strain, in./in.
θ	slope, rad
$\theta_{1,2}$	slope of component 1 at its juncture with component 2, rad
$\theta_{2,1}$	slope of component 2 at its juncture with component 1, rad
λ	$4\sqrt{3(1-\nu^2)}/\sqrt{at}$, in.$^{-1}$
ν	Poisson's ratio
σ	stress, psi
ω	deflection, in.

Subscripts:

r	radial
t	tangential
1, 2, 3	components 1, 2, 3

Superscripts:

b	bottom of plate
t	top of plate
*	equivalent value

APPENDIX B

CALCULATED STRAIN LEVELS

The general solution of the plate problem proceeds as follows:

(1) Assume that the plate is cut into two components, a ring and a plate, as shown in figure 8 (p. 9).

(2) Find an expression for the change in radial displacement and in slope for each component at its common juncture with other components in terms of the known and the unknown loads. (In the case of the friction-locked condition, the radial motion of the cylinder is considered as well.)

(3) Write algebraic equations which express the fact that the slope and the displacement at common junctures between components must be equal.

(4) Solve the equations simultaneously to find the magnitude of the previously unknown loads at the common junctures.

(5) Use the previously unknown loads with the originally known loads to find the strain at various radii.

Two possible conditions exist for the effect of the cylindrical support on the plate: (1) There is a complete lack of friction between the support and the plate (friction free), or (2) the plate does not slide radially on the support edge of the cylinder (friction locked). Two general methods of analysis were employed; the first method used a ligament-efficiency factor to account for the weakening effect of drilled holes, and the second employed material property change. The cases calculated by the efficiency-factor method are designated B-1 and B-2, while those calculated by the material-property-change method are designated A-1 and A-2.

A bracket method of analysis was used to determine the feasibility of modifying the presently available methods of analysis to account for the variable hole sizes. The bracket method is based on the premise that if the plate is assumed to have holes with only the thinnest ligaments, the calculated strains will be of greater magnitude than those measured, whereas the use of the thickest ligaments would yield calculated strains of lower value than the gages indicate. The calculations for the thicker ligaments are designated cases A-1 and B-1, while those for the thinner ligaments are designated cases A-2 and B-2.

Loads

Seven studs were used to load the plate. Six studs were located in a circular pattern about the plate center, while one stud was located at the plate center (fig. 4, p. 5). The studs were tightened until the direct strain on each was 1200 microinches. A test of the

stud material yielded a modulus of elasticity of 32.60×10^6. The studs were 3/8 inch in diameter.

The bolt stress is then

$$\sigma = E\epsilon \tag{B1}$$

The total load for six bolts is

$$P = 6\sigma A \tag{B2}$$

where A is the bolt cross-sectional area or

$$P = 6E\epsilon A = 25\ 924 \text{ lb} \tag{B3}$$

The load imposed by the center bolt is

$$\overline{P} = \frac{P}{6} = 4\ 321 \text{ lb}$$

Motion

The following equations are the general equations for compatibility of motion between portions of the plate and the cylinder (in case of the friction-locked condition only) (fig. 8(b), p. 9). The rotation of component 1 is equal to the rotation of component 2 at the common juncture:

$$\theta_{1,2} = \theta_{2,1} \tag{B4}$$

The radial motion of component 1 is equal to the radial motion of component 2 at the common juncture:

$$\delta_{1,2} = \delta_{2,1} \tag{B5}$$

The radial motion of component 2 is equal to the radial motion of component 3 at the common juncture:

$$\delta_{2,3} = \delta_{3,2} \tag{B6}$$

Equation (B6) is used only with the friction-locked condition. The equations written in their entirety for the friction-free condition are as follows (fig. 8(a)):

Equation (B4):

$$\frac{P(d^2 - b^2)}{4\pi KD^*b(1 + \nu^*)} - \frac{\bar{P}b}{4K(1 + \nu^*)\pi D^*} + \frac{M_{1,2}b}{KD^*(1 + \nu^*)} - \frac{P_{1,2}\bar{b}b}{KD^*(1 + \nu^*)} = \frac{-6(P + \bar{P})(a - b)}{\pi Et_2^3 \ln \frac{c}{b}} - \frac{12bM_{1,2}}{Et_2^3 \ln \frac{c}{b}} \tag{B7}$$

In the compatibility equations, the first term in equations (B7) and (B9) is obtained by taking the derivative with respect to r of equation (f) or equation (77) of reference 8 (p. 64). The second term in equations (B7) and (B9) is obtained by taking the derivative of equation (a) or equation (89) of reference 8 (p. 68) and then letting $r = b$. The third and fourth terms in equations (B7) and (B9) are obtained from equation (b) of reference 8 (p. 68) by letting $M_{1,2} = M$ and $P_{1,2}\bar{b} = M$. The right sides of equations (B7) and (B9) are modified versions of equation (163) of reference 9 (p. 179).

Equation (B5):

$$\frac{-P\bar{b}(d^2 - b^2)}{4K\pi D^*b(1 + \nu^*)} + \frac{Pb\bar{b}}{4K\pi D^*(1 + \nu^*)} - \frac{M_{1,2}\bar{b}}{KD^*(1 + \nu^*)}$$

$$+ P_{1,2}\left[\frac{b\bar{b}^2}{KD^*(1 + \nu^*)} + \frac{b(1 - \nu^*)}{KE^*t}\right] = \frac{-P_{1,2}b}{Et_2}\left(\frac{c^2 + b^2}{c^2 - b^2} + \nu\right) \tag{B8}$$

In equations (B8) and (B10), the first three terms left of the equal sign are the first three terms in equation (B7) multiplied by a distance to yield radial motion due to rotation. The fourth term consists of two parts; the first part is rotation multiplied by distance, and the second part is from equation (209) of reference 9, where the inside radius is assumed to be 0. The term to the right of the equal sign in equations (B8) and (B10) is obtained from equation (208) of reference 9 (p. 241).

The compatibility equations of motion for the friction-locked condition are as follows (fig. 8(b)):

Rotation at juncture of component 1 with component 2:

$$\frac{P(d^2 - b^2)}{4\pi KD^*b(1 + \nu^*)} - \frac{\overline{P}b}{4K(1 + \nu^*)\pi D^*} + \frac{M_{1,2}b}{Kd^*(1 + \nu^*)} - \frac{P_{1,2}b\bar{b}}{KD^*(1 + \nu^*)}$$

$$= \frac{-6(P + \overline{P})(a - b)}{\pi Et_2^3 \ln \frac{c}{b}} - \frac{12bM_{1,2}}{Et_2^3 \ln \frac{c}{b}} + \frac{6P_{2,3}t_2a}{Et_2^3 \ln \frac{c}{b}} \qquad \text{(B9)}$$

Displacement at juncture of component 1 with component 2:

$$\frac{-\overline{P}(d^2 - b^2)\bar{b}}{4\pi KD^*b(1 - \nu^*)} + \frac{\overline{P}b\bar{b}}{4\pi KD^*(1 + \nu^*)} - \frac{M_{1,2}b\bar{b}}{KD^*(1 + \nu^*)} + \frac{P_{1,2}}{K}\left[\frac{b\bar{b}^2}{D^*(1 + \nu^*)} + \frac{b(1 - \nu^*)}{E^*t}\right]$$

$$= \frac{-P_{1,2}b}{Et_2}\left(\frac{c^2 + b^2}{c^2 - b^2} + \nu\right) - \frac{bP_{2,3}}{Et_2(c^2 - b^2)}\left[c^2(1 + \nu) + a^2(1 - \nu)\right] \qquad \text{(B10)}$$

Displacement at juncture of component 3 with component 2:

$$\frac{2P_{2,3}\lambda}{\overline{K}} = -\frac{P_{2,3}}{2aEt_2(c^2 - b^2)}\left\{\left[a^2(1 - \nu) + c^2(1 + \nu)\right]\left[a^2(1 - \nu) + b^2(1 + \nu)\right]\right\}$$

$$- \frac{t_2}{2}\left[\frac{6P_{2,3}at_2}{Et_2^3 \ln \frac{c}{b}} - \frac{6(P + \overline{P})(a - b)}{\pi Et_2^3 \ln \frac{c}{b}} - \frac{12bM_{1,2}}{Et_2^3 \ln \frac{c}{b}}\right] - \frac{b^2P_{1,2}}{Eat_2(c^2 - b^2)}\left[(1 - \nu)a^2 + (1 + \nu)c^2\right] \qquad \text{(B11)}$$

In the preceding equations, K = 1 (where K is an efficiency factor) if cases A-1 and A-2 are being evaluated. If cases B-1 and B-2 are being calculated, let $D^* = D$, $\nu^* = \nu$, $E^* = E$, and K is a calculated value.

The second term to the right of the equal sign in equation (B10) and the first term to the right of the equal sign of equation (B11) are obtained by a special derivation explained in appendix C. The last term to the right of the equal sign in equation (B11) is equation (207) of reference 9 (p. 240). The term to the left of the equal sign in equation (B11) is obtained directly from equation (39a) of reference 10 (p. 52). The second term to the right of the equal sign in equation (B11) is the radial motion of component 2 due to rotation and is slightly modified from the basic formulas of equation (163) of reference 9 (p. 179). The simultaneous solution of equations (B7) and (B8) for the friction-free con-

dition and equations (B9) to (B11) for the friction-locked condition yields the desired values for the unknown discontinuity forces.

The strains at any radius desired can then be obtained by substitution into the following equations, which are derived in appendix C.

$$\epsilon_r^t = \frac{Y(1-\nu^*)}{KE^*t^2}\left\{P_{1,2}t + 6(M_{1,2} - P_{1,2}\bar{b}) + \frac{P}{4\pi}\left[7\nu^* - 3(1+\nu^*)\frac{d^2}{r^2} + 3(1-\nu^*)\frac{d^2}{b^2} - 7(1+\nu^*)\ln\frac{b}{r}\right]\right\} \quad \text{(B13)}$$

$$\epsilon_r^b = \frac{Y(1-\nu^*)}{KE^*t^2}\left\{P_{1,2}t - 6(M_{1,2} - P_{1,2}\bar{b}) - \frac{P}{4\pi}\left[7\nu^* - 3(1+\nu^*)\frac{d^2}{r^2} + 3(1-\nu^*)\frac{d^2}{b^2} - 7(1+\nu^*)\ln\frac{b}{r}\right]\right\} \quad \text{(B14)}$$

$$\epsilon_t^t = \frac{Y(1-\nu^*)}{KE^*t^2}\left\{P_{1,2}t + 6(M_{1,2} - P_{1,2}\bar{b}) + \frac{P}{4\pi}\left[3(1+\nu^*)\frac{d^2}{r^2} - 7(1+\nu^*)\ln\frac{b}{r} + 3(1-\nu^*)\frac{d^2}{b^2} - 7\right]\right\} \quad \text{(B15)}$$

$$\epsilon_t^b = \frac{Y(1-\nu^*)}{KE^*t^2}\left\{P_{1,2}t - 6(M_{1,2} - P_{1,2}\bar{b}) - \frac{P}{4\pi}\left[3(1+\nu^*)\frac{d^2}{r^2} - 7(1+\nu^*)\ln\frac{b}{r} + 3(1-\nu^*)\frac{d^2}{b^2} - 7\right]\right\} \quad \text{(B16)}$$

The same restrictions for the use of D^*, ν^*, E^*, and K apply in these equations as for equations (B7) to (B11).

The substitution of values into equations (B13) to (B16) yields the radial and the tangential strains for direct comparison with those measured by the strain gages.

The equivalent elastic properties for use with cases A-1 and A-2 are found through the use of figure 5 of reference 7. For cases A-1 and A-2, h/R is determined and

E^*/E and ν^* are obtained from reference 7. Since figure 5 in reference 7 is for steel, the value of ν^* obtained from this figure is multiplied by the ratio of Poisson's ratio for aluminum to that for steel to obtain the desired value of ν^*.

The ligament-efficiency method is defined in reference 3 (p. 319). This efficiency factor is modified for use with either case B-1 or B-2 as follows:

$$K = \frac{2R - d_3}{2R} \tag{B17}$$

APPENDIX C

DERIVATION OF INFLUENCE FACTORS AND STRAIN EQUATIONS

The first term in equation (B11) on the right side of the equal sign and the last term in equation (B10) are obtained in the following manner: If ring 2 in figure 10 is assumed to be cut by a circumferential plane at radius a as shown, then the entire load $P_{2,3}$ can be originally placed on subring 2A. A radial gap will then open at radius a between subrings 2A and 2B. In order to close this gap, a restoring pressure P_x must then exist between subrings 2A and 2B. The pressure load on subring 2A is then $(P_{2,3}/t_2) - P_x$, while on subring 2B the pressure load is approximately P_x; both pressure loads are located at radius a.

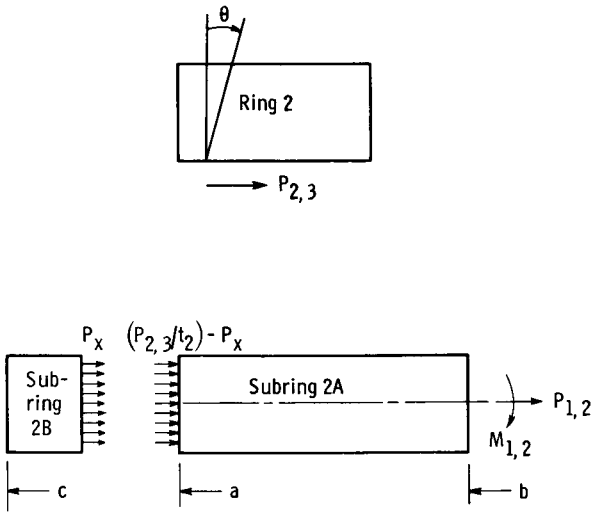

Figure 10. - Partitioning of support ring for determination of influence factors.

The algebraic statement that the radial motion at radius a between the subrings must be equal furnishes an equation for determining P_x. This equation is

$$\frac{-aP_x}{E}\left(\frac{a^2 + c^2}{c^2 - a^2} + \nu\right) = \frac{-a\left(\frac{P_{2,3}}{t_2} - P_x\right)}{E}\left(\frac{b^2 + a^2}{a^2 - b^2} - \nu\right) \tag{C1}$$

Both equations are in reference 9 (p. 241). The term on the left side is equation (208), while that on the right side is equation (209). Equation (C1) yields a numerical value for the unknown pressure P_x.

$$P_x = \frac{P_{2,3}\left[(b^2 + a^2) - \nu(a^2 - b^2)\right](c^2 - a^2)}{2a^2 t_2 (c^2 - b^2)} \tag{C2}$$

The substitution of equation (C2) into the left side of equation (C1) yields the displacement of ring 2 at radius a, which is the first term to the right of the equal sign in equa-

tion (B11). The substitution of equation (C2) into equation (207) of reference 9 (p. 240) yields the displacement of ring 2 at radius b, which is the last term in equation (B10).

The derivation for the basic strain equations is as follows:

From two-dimensional Hooke's law,

$$\epsilon_r = \frac{1}{E^*}(\sigma_r - \nu^*\sigma_t) \tag{C3}$$

$$\epsilon_t = \frac{1}{E^*}(\sigma_t - \nu^*\sigma_r) \tag{C4}$$

The stress in the plate in the radial and the tangential directions can be described by the following equation:

$$\sigma_r^t = \frac{Y}{K}\left\{\frac{P_{1,2}}{t} + \frac{6}{t^2}(M_{1,2} - P_{1,2}\bar{b}) - \frac{3P}{2\pi t^2}\left[(1+\nu^*)\ln\frac{b}{r} + (1-\nu^*)\frac{d^2}{2r^2} - (1-\nu^*)\frac{d^2}{2d^2}\right] - \frac{3P}{2\pi t^2}(1+\nu^*)\ln\frac{b}{r}\right\} \tag{C5}$$

$$\sigma_r^b = \frac{Y}{K}\left\{\frac{P_{1,2}}{t} - \frac{6}{t^2}(M_{1,2} - P_{1,2}\bar{b}) + \frac{3P}{2\pi t^2}\left[(1+\nu^*)\ln\frac{b}{r} + (1-\nu^*)\frac{d^2}{2r^2} - (1-\nu^*)\frac{d^2}{2b^2}\right] + \frac{3\bar{P}}{2\pi t^2}(1+\nu^*)\ln\frac{b}{r}\right\} \tag{C6}$$

$$\sigma_t^t = \frac{Y}{K}\left\{\frac{P_{1,2}}{t} + \frac{6}{t^2}(M_{1,2} - P_{1,2}\bar{b}) - \frac{3P}{2\pi t^2}\left[(1-\nu^*) + (1+\nu^*)\ln\frac{b}{r} - (1-\nu^*)\frac{d^2}{2r^2} - (1-\nu^*)\frac{d^2}{2b^2}\right] - \frac{3\bar{P}}{2\pi t^2}\left[(1+\nu^*)\ln\frac{b}{r} + (1-\nu^*)\right]\right\} \tag{C7}$$

$$\sigma_t^b = \frac{Y}{K}\left\{\frac{P_{1,2}}{t^2} - \frac{6}{t^2}(M_{1,2} - P_{1,2}\bar{b}) + \frac{3P}{2\pi t^2}\left[(1 - \nu^*) + (1 + \nu^*)\ln\frac{b}{r}\right.\right.$$

$$\left.\left. - (1 - \nu^*)\frac{d^2}{2r^2} - (1 - \nu^*)\frac{d^2}{2b^2}\right] + \frac{3\bar{P}}{2\pi t^2}(1 + \nu^*)\ln\frac{b}{r} + (1 - \nu^*)\right\} \qquad \text{(C8)}$$

With $\bar{P} = P/6$, the substitution of equations (C5) and (C7) into equations (C3) and (C4), and the substitution of equations (C6) and (C8) into equations (C3) and (C4), the basic strain equations (B13) to (B16) are obtained.

In equations (C5) to (C8), the terms used were obtained as follows: The terms

$$\frac{P_{1,2}}{t} \qquad \text{(ref. 9, p. 239, eq. (200))}$$

$$\frac{6}{t^2}(M_{1,2} - P_{1,2}\bar{b}) \qquad \text{(ref. 11, p. 191, case 3)}$$

$$\frac{3P}{2\pi t^2}\left[(1 + \nu^*)\ln\frac{b}{r} + (1 - \nu^*)\frac{d^2}{2r^2} - (1 - \nu^*)\frac{d^2}{2b^2}\right]$$

and

$$\frac{3P}{2\pi t^2}\left[(1 - \nu^*) + (1 + \nu^*)\ln\frac{b}{r} - (1 - \nu^*)\frac{d^2}{2r^2} - (1 - \nu^*)\frac{d^2}{2b^2}\right]$$

are obtained from the general equations

$$\left.\begin{aligned}\sigma_r &= \frac{6M_r}{t^2}\\ \text{and}\qquad\\ \sigma_t &= \frac{6M_t}{t^2}\end{aligned}\right\} \qquad \text{(C9)}$$

where

$$\left.\begin{aligned} M_r &= -D^*\left(\frac{d^2\omega}{dr^2} + \frac{\nu}{r}\frac{d\omega}{dr}\right) \\ \text{and} \\ M_t &= -D\left(\frac{1}{r}\frac{d\omega}{dr} + \frac{\nu d^2\omega}{dr^2}\right) \end{aligned}\right\} \qquad \text{(C10)}$$

(ref. 8, p. 52, eqs. (52) and (53)). The ω in equations (C10) is in reference 8 (p. 64, eq. (77)) or in reference 11 (p. 191, case 3).

For the terms

$$\left.\begin{aligned} \sigma_r &= \frac{3\overline{P}}{2\pi t^2}(1 + \nu^*)\ln\frac{b}{r} \\ \text{and} \\ \sigma_t &= \frac{3\overline{P}}{2\pi t^2}\left[(1 + \nu^*)\ln\frac{b}{r} + (1 - \nu^*)\right] \end{aligned}\right\} \qquad \text{(C11)}$$

equations (C9) are used with M_t and M_r from reference 8 (p. 68, eqs. (90) and (91)) or reference 11 (p. 191, case 2).

REFERENCES

1. Horvay, G.: The Plane-Stress Problem of Perforated Plates. J. Appl. Mech., vol. 19, no. 3, Sept. 1952, pp. 355-360.
2. Gardner, K. A.: Heat-Exchanger Tube-Sheet Design. J. Appl. Mech., vol. 15, no. 4, Dec. 1948, pp. 377-385.
3. Miller, K. A. G.: The Design of Tube Plates in Heat Exchangers. Inst. Mech. Eng. Proc., vol. 1B, no. 6, 1952, pp. 215-231.
4. Duncan, J. P.: The Structural Efficiency of Tube-Plates for Heat Exchangers. Inst. Mech. Eng. Proc., vol. 169, 1955, pp. 789-802.
5. Sampson, R. C.: Photoelastic Frozen Stress Study of the Effective Elastic Constants of Perforated Materials. Rep. No. WAPD-DLE-319, Westinghouse Research Laboratories, May 29, 1959.
6. Leven, M. M.: Photoelastic Determination of Stresses in Tube Sheets and Comparison with Calculated Values. Bettis Tech. Rev., WAPD-BT-18, Apr. 1960, pp. 53-73.
7. O'Donnell, W. J.; and Langer, B. F.: Design of Perforated Plates. J. Eng. Industry, vol. 84, no. 3, Aug. 1962, pp. 307-320.
8. Timoshenko, S.; and Woinowsky-Krieger, S.: Theory of Plates and Shells. Second ed., McGraw-Hill Book Co., Inc., 1959.
9. Timoshenko, S.: Strength of Materials. Vol. II, 2nd ed., D. Van Nostrand Co., Inc., 1941.
10. Hetényi, M.: Beams on Elastic Foundation. University of Michigan Press, 1946.
11. Roark, Raymond J.: Formulas for Stress and Strain. 2nd ed., McGraw-Hill Book Co., Inc., 1943.

[redacted]

"The aeronautical and space activities of the United States shall be conducted so as to contribute . . . to the expansion of human knowledge of phenomena in the atmosphere and space. The Administration shall provide for the widest practicable and appropriate dissemination of information concerning its activities and the results thereof."

—NATIONAL AERONAUTICS AND SPACE ACT OF 1958

NASA SCIENTIFIC AND TECHNICAL PUBLICATIONS

TECHNICAL REPORTS: Scientific and technical information considered important, complete, and a lasting contribution to existing knowledge.

TECHNICAL NOTES: Information less broad in scope but nevertheless of importance as a contribution to existing knowledge.

TECHNICAL MEMORANDUMS: Information receiving limited distribution because of preliminary data, security classification, or other reasons.

CONTRACTOR REPORTS: Technical information generated in connection with a NASA contract or grant and released under NASA auspices.

TECHNICAL TRANSLATIONS: Information published in a foreign language considered to merit NASA distribution in English.

TECHNICAL REPRINTS: Information derived from NASA activities and initially published in the form of journal articles.

SPECIAL PUBLICATIONS: Information derived from or of value to NASA activities but not necessarily reporting the results of individual NASA-programmed scientific efforts. Publications include conference proceedings, monographs, data compilations, handbooks, sourcebooks, and special bibliographies.

Details on the availability of these publications may be obtained from:

SCIENTIFIC AND TECHNICAL INFORMATION DIVISION

NATIONAL AERONAUTICS AND SPACE ADMINISTRATION

Washington, D.C. 20546

[redacted]